Water cycling in a Bornean tropical rain forest under current and projected precipitation scenarios

Tomo'omi Kumagai,[1,2] Gabriel G. Katul,[3] Taku M. Saitoh,[4] Yoshinobu Sato,[4] Odair J. Manfroi,[5] Toshiyuki Morooka,[5] Tomoaki Ichie,[6] Koichiro Kuraji,[5] Masakazu Suzuki,[5] and Amilcare Porporato[7,8]

Received 31 March 2003; revised 9 October 2003; accepted 12 November 2003; published 17 January 2004.

[1] Southeastern Asian tropical rain forests are among the most important biomes in terms of annual productivity and water cycling. How their hydrologic budgets are altered by projected shifts in precipitation is examined using a combination of field measurements, global climate model (GCM) simulation output, and a simplified hydrologic model. The simplified hydrologic model is developed with its primary forcing term being rainfall statistics. A main novelty in this analysis is that the effects of increased (or decreased) precipitation on increased (or decreased) cloud cover and hence evapotranspiration is explicitly considered. The model is validated against field measurements conducted in a tropical rain forest in Sarawak, Malaysia. It is demonstrated that the model reproduces the probability density function of soil moisture content (s), transpiration (T_r), interception (I_c), and leakage loss (Q). On the basis of this model and projected shifts in precipitation statistics by GCM the probability distribution of I_c, Q and, to a lesser extent, s varied appreciably at seasonal timescales. The probability distribution of T_r was least impacted by projected shifts in precipitation. *INDEX TERMS:* 1655 Global Change: Water cycles (1836); 1869 Hydrology: Stochastic processes; 1866 Hydrology: Soil moisture; 1818 Hydrology: Evapotranspiration; *KEYWORDS:* eddy covariance, evapotranspiration, soil moisture, stochastic process, tropical rainforest, water cycling

Citation: Kumagai, T., G. G. Katul, T. M. Saitoh, Y. Sato, O. J. Manfroi, T. Morooka, T. Ichie, K. Kuraji, M. Suzuki, and A. Porporato (2004), Water cycling in a Bornean tropical rain forest under current and projected precipitation scenarios, *Water Resour. Res.*, *40*, W01104, doi:10.1029/2003WR002226.

1. Introduction

[2] The projected growth in atmospheric greenhouse gases within the coming century, as summarized by the Intergovernmental Panel on Climate Change report [e.g., *Houghton et al.*, 2001], will significantly impact global and regional temperatures with concomitant modifications to precipitation patterns. Tropical rain forests are among the most important biomes in terms of annual primary productivity and water cycling; hence, assessing their sensitivity to potential shifts in precipitation patterns is a necessary first step to quantifying future local, regional, and global water cycling. Although these forests now cover only 12% of the total land surface [*Food and Agricultural Organization*, 1993], they contain about 40% of the carbon in the terrestrial biosphere [*Skole and Tucker*, 1993] and are responsible for about 50% of terrestrial gross primary productivity [*Grace et al.*, 2001]. Also, tropical rain forests are a major source of global land surface evaporation [*Choudhury et al.*, 1998] with profound influences on both global and regional climate and hydrological cycling [e.g., *Lean and Warrilow*, 1989; *Nobre et al.*, 1991]. This large latent energy flux from tropical rain forests is known to influence global atmospheric circulation patterns [*Paegle*, 1987].

[3] A number of field studies reported the components of the hydrologic cycle in Amazonian tropical rain forests [e.g., *Shuttleworth et al.*, 1984; *Hodnett et al.*, 1995; *Grace et al.*, 1995; *Malhi et al.*, 2002; *Vourlitis et al.*, 2002]. These studies suggest that 50% of incident precipitation is recycled as evapotranspiration.

[4] What is less certain is water cycling in Southeast Asian tropical rain forests, the subject of this investigation. As *Dykes* [1997] pointed out, detailed long-term studies on the hydrological components are needed in the "maritime" environments of Southeast Asia because of the prominent effect of El Niño-Southern Oscillation (ENSO).

[5] Our goal is to investigate how water cycling of a lowland dipterocarp forest in Southeast Asian humid tropics will respond to current and projected precipitation patterns. Toward this goal, we use global climate model (GCM) simulation outputs of current and future precipitation sta-

[1]University Forest in Miyazaki, Kyushu University, Shiiba-son, Miyazaki, Japan.
[2]Also at Nicholas School of the Environment, Duke University, Durham, North Carolina, USA.
[3]Nicholas School of the Environment, Duke University, Durham, North Carolina, USA.
[4]Research Institute of Kyushu University Forest, Fukuoka, Japan.
[5]Graduate School of Agricultural and Life Sciences, University of Tokyo, Tokyo, Japan.
[6]Field Science Center for Northern Biosphere, Hokkaido University, Sapporo, Japan.
[7]Department of Civil and Environmental Engineering, Duke University, Durham, North Carolina, USA.
[8]Also at Dipartimento di Idraulica, Trasporti ed Infrastrutture Civili, Politecnico di Torino, Torino, Italy.

0043-1397/04/2003WR002226$09.00

tistics, a simplified hydrological model described by *Rodriguez-Iturbe et al.* [1999], *Laio et al.* [2001], and *Porporato et al.* [2002], and detailed field measurements conducted over a 2-year period. Prior to assessing the hydrologic budget for future precipitation scenarios, the model is first validated with field measurements conducted in a tropical rain forest in Lambir Hills National Park, Sarawak, Malaysia, over a 2-year period, described next.

2. Study Site and Measurements

2.1. Site Description

[6] The experiment was carried out in a natural forest in Lambir Hills National Park (4°12′N, 114°02′E), 30 km south of Miri City, Sarawak, Malaysia (Figure 1). The mean annual rainfall at Miri Airport, 20 km from the study site, for the period 1968–2001 was around 2740 mm with some seasonal variation. For example, the mean rainfall for September-October-November (SON) was around 880 mm and for March-April-May (MAM) was around 520 mm. For the period 1999–2001, the mean monthly number of rain days ranged from 10 in August 2001 to 27 in January 2001. The average rainfall per rain day ranged from 7.2 mm in August 2001 to 21.3 mm in January 2001. The mean annual temperature is around 27°C with minor seasonal variation [e.g., *Yamakura et al.*, 1995].

[7] The rain forest in this park consists of two types of original vegetation common to the whole of Borneo, i.e., mixed dipterocarp forest and tropical heath forest [*Yamakura et al.*, 1995]. The former contains various types of dipterocarp trees, which cover 85% of the total park area. The soils consist of red-yellow podzonic soils (Malaysian classification) or ultisols (USDA Soil Texonomy), with a high sand content (62–72%), an accumulation of nutrient content at the surface horizon, a low pH (4.0–4.3), and a high porosity (54–68%) [*Ishizuka et al.*, 1998; *Sakurai*, 1999]. Borneo is covered primarily by hilly topography and most of its soil type is ultisol. Ultisol is a typical soil of much of Southeast Asia, and its distribution corresponds to that of lowland and hill dipterocarp forest [*Ohta and Effendi*, 1992].

2.2. Crane Facility

[8] A 4 ha experimental plot at an altitude of 200 m and on a gentle slope (<5°), gridded in 400 subplots or quadrats of 10×10 m^2, was used in this project. An 80-m-tall (at the base of the gondola) canopy crane with a 75-m-length rotating jib was constructed in the center of this plot to provide access to the upper canopy. Observational stages at 4 levels (23.5, 38.5, 59.0, and 75.5 m above the ground) accessible by an elevator were also installed. One stage (59.0 m high) was devoted to eddy covariance flux measurements. The subplots or quadrats were used for in-canopy micrometeorological measurements, and throughfall and stemflow measurements. The canopy height surrounding the crane is about 40 m but the height of emergent treetops can reach up to 50 m.

2.3. Leaf Area Measurements

[9] The leaf area index (LAI) was measured in 2002 using a pair of plant canopy analyzers (LAI-2000, Li-Cor, Lincoln, NE) every 5 m on a 30×30 m^2 subplot. The LAI ranged from 4.8 to 6.8 m^{2}m^{-2} with a mean of 6.2 m^{2}m^{-2} (M. Yamashita, unpublished data). The amount of litterfall in each month were evenly distributed throughout the year (M. Nakagawa, unpublished data) perhaps suggesting little variations in LAI.

2.4. Micrometeorological and Soil Moisture Measurements

[10] The following instruments were installed at the top of the crane, 85.8 m from the forest floor: a solar radiometer (MS401, EKO, Tokyo, Japan), an infrared radiometer (Model PIR, Epply, Newport, RI), and a tipping bucket rain gauge (RS102, Ogasawara Keiki, Tokyo, Japan). At a separate tower located some 100 m south from the crane, the upward short-wave radiation and long-wave radiation were measured using a solar radiometer (CM06E, Kipp & Zonen, Delft, Netherlands) and an infrared radiometer (Model PIR, Epply, Newport, RI) installed upside down since 15 December 2001. Samples for radiation were taken every 5 s and an averaging period of 10 min was used (CR10X datalogger, Campbell Scientific, Logan, UT). These measurements were used to compute net radiation (R_n; W m^{-2}). The net radiation time series prior to 15 December 2001 were calculated using the relationship between solar radiation (R_s; W m^{-2}) and net radiation ($R_n = 0.87R_s - 35.0$, $R^2 = 0.99$). Maximum and average total daily solar radiation during the measurement period were 24.9 and 17.0 MJ m^{-2} d^{-1}, respectively, and maximum and average total daily net radiation were 18.6 and 11.8 MJ m^{-2} d^{-1}, respectively.

[11] Volumetric soil moisture content (θ) and matric potential (ψ) were measured in a subplot at 10, 20 and 50 cm below the forest floor at 10-min intervals (CR23X datalogger, Campbell Scientific, Logan, UT). A time domain reflectometer (TDR; CS615, Campbell Scientific, Logan, UT) was used to measure the time series of θ. A tensiometer (DIK3150, Daiki, Tokyo, Japan) was also used to monitor ψ at the same depth as θ thereby providing the necessary measurements to compute in-situ soil water retention curves at each depth. The weighted average θ in the 0–50 cm soil layer was calculated as $\theta = (15\theta_{10} + 20\theta_{20} + 15\theta_{50})/50$ (where θ_{10}, θ_{20} and θ_{50} are volumetric soil moisture content at depths of 10, 20 and 50 cm, respectively, in m^{3}m^{-3}). The relative extractable water in the soil (Θ; m^{3}m^{-3}) was calculated using this average θ as: $(\theta - \theta_r)/(\theta_s - \theta_r)$, where θ_s and θ_r are the saturated water content and the residual water content averaged in the 0–50 cm, respectively. The θ_s and θ_r were taken as the maximum and minimum observed θ during the experimental period (17 March 2001 to 31 May 2002). The Θ ranges from 0 (soil dry) to 1 (soil saturated). As a result, the relation $\Theta = 0.0095\,s - 0.712$ (where s is the soil moisture content (mm) over the 0–50 cm soil layer) was obtained here.

2.5. Evapotranspiration Measurements by the Eddy Covariance Method

[12] A three-dimensional sonic anemometer (DA-600, Kaijo, Tokyo, Japan) was installed at 60.2 m, i.e., 20 m above the mean canopy height. Co-located with the sonic anemometer is an open-path CO_2/H_2O analyzer (LI-7500, Li-Cor, Lincoln, NE) placed about 30 cm away. There was, in addition, a ventilated psycrometer (MS020S, EKO, Tokyo, Japan) installed adjacent to the sonic anemometer and an open path analyzer for calibration and correction for density effects [*Webb et al.*, 1980]. Wind speeds and gas concentra-

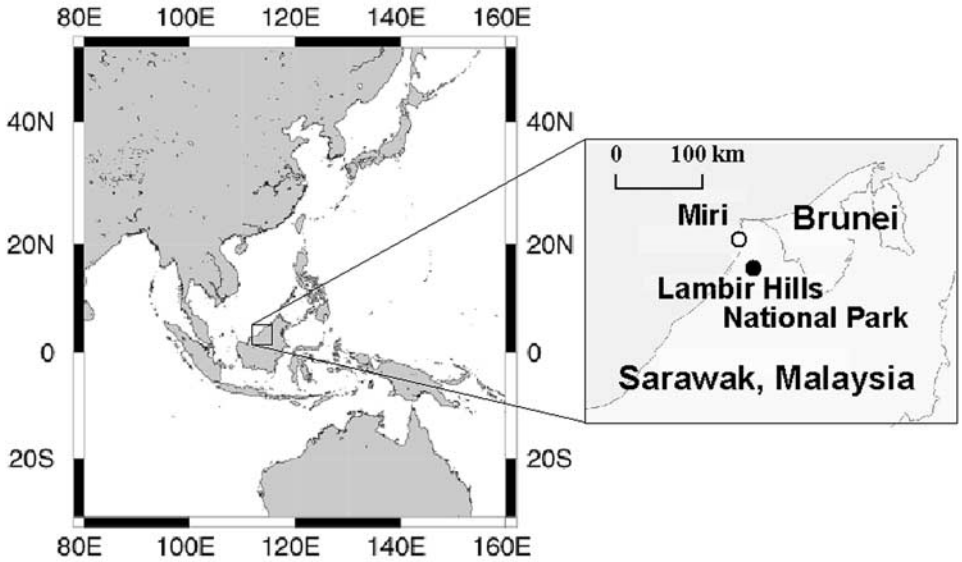

Figure 1. Location of Lambir Hills National Park, Sarawak, Malaysia.

tion time series were all sampled at 10 Hz. All variances and co-variances required for eddy covariance flux estimates were computed over a 30-min averaging interval. For the flux calculations, time series were de-trended using a moving-average time constant of 200 s and the wind field (u, v, w) coordinates were rotated so that the mean v and w were zero over 10 min periods. Fluxes measured during rain events were discarded. Details on the eddy covariance measurement are presented by *Kumagai et al.* [2004]. Maximum and average daily transpiration rates during the measurement period, resulting from water vapor flux data when the canopy was dry, were 4.99 and 2.75 mm d^{-1}, respectively.

[13] At the study site, precipitation, solar radiation, and air temperature have small seasonal variations. However, intraannual dry spells have been reported [*Kumagai et al.*, 2004]. As the intraannual dry spells occur regularly throughout the year, transpiration rate is likely to be overly sensitive to the soil moisture condition. We will later discuss the dependency of transpiration rate on soil moisture condition.

2.6. Throughfall and Stemflow Measurements

[14] A plot representative of the 4 ha experimental plot was instrumented for throughfall and stemflow measurements. Throughfall was measured with 40 collectors, 20 of which were dispersed on a grid over the fixed plot. The collectors used for throughfall measurement were manually operated gauges assembled with 20.6-cm diameter plastic funnels and 10-L capacity bottles. Samples were manually taken every weekday and Saturday between 8:00 and 13:00 LST using 1-L plastic cylinders with 10-mL graduation intervals.

[15] Collars around the trunks were connected to 30-L bottles or 15.7 cc tipping bucket flowmeters (No.34, Ohta Keiki, Tokyo, Japan) allowed stemflow measurement on 81 trees of various circumferences (ranging between 1 and 130 cm). 78 of those trees were located inside the fixed plot and 3 outside. Some of the stemflow measurements were sampled as the time-of-tip by event data logger (KADEC-UP, Kona System, Sapporo, Japan) and the other were measured manually using the same procedure as throughfall measurements. Details on throughfall and stemflow measurements are presented by *Manfroi et al.* [2004].

3. Methodology

[16] We discuss first the hydrologic model development, parameterization, and testing for this experiment, and then proceed to discuss its usage for assessing shifts in the hydrologic components following projected shifts in precipitation statistics. For the model testing, precipitation time series was measured and was used to drive the model calculations; however, in our model simulations for future climates – only precipitation statistics are available thereby necessitating a stochastic treatment. The generation of stochastic precipitation time series, and the connections to GCM simulation outputs are also discussed.

3.1. Hydrologic Model

[17] For gentle slopes, lateral movement can be neglected, and the vertically integrated continuity equation is given by

$$\frac{ds}{dt} = P - T_r - I_c - Q, \tag{1}$$

where t is the time (day), P the precipitation (mm d^{-1}), T_r the transpiration (mm d^{-1}), I_c the interception (mm d^{-1}) and Q the leakage loss (mm d^{-1}) from the soil layer. Given that the root zone is shallow, we assume that the top 50 cm soil layer captures much of the root zone water uptake activity. This model is analogous to the model used by *Wood et al.* [1992] for planar homogeneous soil conditions. Also, we assume that Q includes runoff and that soil evaporation is insignificant when compared to the total transpiration flux (given the high LAI at the site) [e.g., *Kelliher et al.*, 1995].

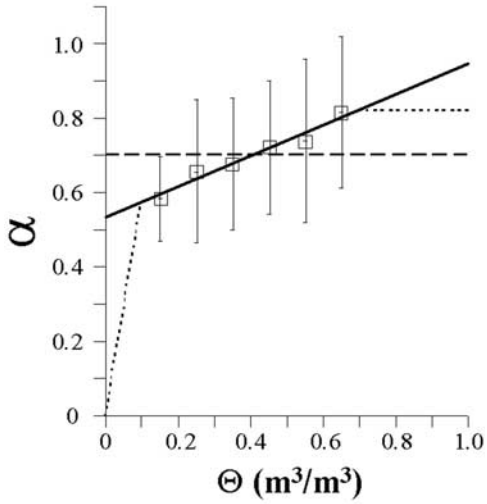

Figure 2. The relationships between the Priestly-Taylor alpha (α) and the relative extractable water in the soil (Θ). The data were averaged in bins of Θ = 0.1 (open square). Vertical bars represent one standard deviation. Solid line represents the model described by equation (3a), dotted line represents the model described by equation (3b), and dashed line represents the model described by equation (3c).

The parameterizations of T_r, I_c, and Q for the site are described next.

3.2. Transpiration Modeling

[18] The primary forcing variable for transpiration in the tropics is net available energy. Hence, we use a modified *Priestly and Taylor* [1972] expression to compute daily transpiration rate T_r (mmd^{-1}) given by:

$$T_r = 86400 \times 1000 \times \alpha \frac{\Delta}{L\rho_w(\Delta+\gamma)} R'_n, \qquad (2)$$

where α is the Priestly-Taylor coefficient, Δ the rate of change of saturation water vapor pressure with temperature (PaK^{-1}), L the latent heat of vaporization of water (J kg^{-1}), ρ_w the density of water (1000 kg m^{-3}), γ the psychrometric constant (66.5 Pa K^{-1}), and R'_n is the daily net radiation above the canopy (W m^{-2}). Thermodynamic variables Δ and L are calculated based on mean air temperature averaged over daylight hours. Daily net radiation was obtained by averaging hourly values.

[19] A major uncertainty in this model is α which, for forested ecosystems, is usually less than its typical 1.26 value because of additional boundary layer, leaf, xylem, and root resistances. We used the eddy covariance measured T_r to obtain daily α, and then proceeded to derive a relationship between Θ and daily α. Here, averaged α was computed in bins of Θ (incremented in 0.1) and a regression model describing Θ and bin-averaged α was derived (R^2 = 0.96) (Figure 2). The values of α obtained here range from 0.6 to 0.8 and appear reasonable when compared to other dry canopy studies [*De Bruin*, 1983]. The bin-averaged α for $0 \le \Theta < 0.1$ and $0.7 < \Theta \le 1.0$ were not well resolved by our measurements. Hence we assumed the following (Figure 2):

$$\alpha = 0.41\Theta + 0.53, \quad \text{for} \quad 0 \le \Theta \le 1.0 \qquad (3a)$$

and

$$\alpha = \begin{cases} 0.057\Theta, & \text{for} \quad 0 \le \Theta < 0.1 \\ 0.41\Theta + 0.53, & \text{for} \quad 0.1 \le \Theta \le 0.7 \\ 0.82, & \text{for} \quad 0.7 < \Theta \le 1.0 \end{cases}. \qquad (3b)$$

That is, α abruptly decreases in severe dry condition and has a constant value for wet conditions. Given the limited range in α, we also investigated the use of a constant α for the entire range of Θ, (Figure 2):

$$\alpha = 0.70, \quad \text{for} \quad 0 \le \Theta \le 1.0. \qquad (3c)$$

The constant α of 0.70 was obtained by averaging all α values for $0 \le \Theta \le 1.0$. We will assess which of these three α models best reproduces the measured T_r.

3.3. Interception Modeling

[20] The relationships between incident rainfall in a single storm event (P'; mm), throughfall (TF; mm), and stemflow (SF; mm) were used to compute rainfall interception. The linear regression equations TF = $0.87P' - 0.78$ (R^2 = 0.99, n = 52) and SF = $0.046\ P' - 0.18$ (R^2 = 0.96, n = 52), shown in Figure 3, were derived from our measurements [*Manfroi et al.*, 2004]. Throughfall only occurred when rainfall exceeded a threshold 0.9 mm while stemflow occurred when rainfall exceeded 3.9 mm.

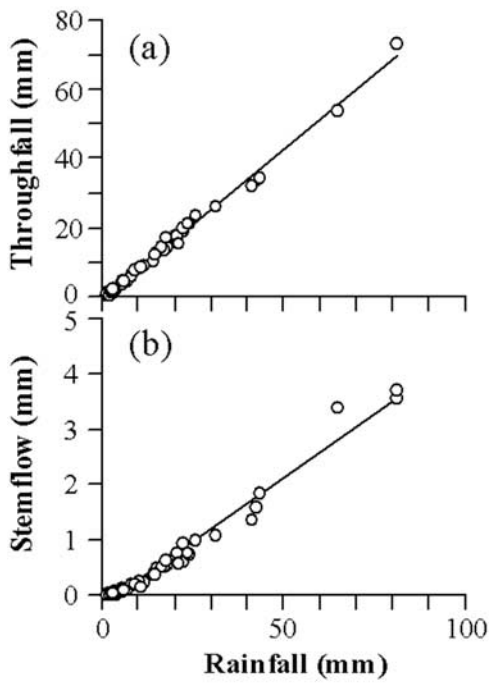

Figure 3. The relationships between (a) stand throughfall (TF) and (b) stand stemflow (SF) and storm rainfall, P', each data point corresponding to a single storm measurement (n = 52). The solid lines are determined from least squares, linear regression; TF = $0.87P' - 0.78$, R^2 = 0.99 (Figure 3a) and SF = $0.046\ P' - 0.18$, R^2 = 0.96 (Figure 3b).

[21] Daily interception I_c was related to rainfall P after subtracting both TF and SF from P to give:

$$I_c = \begin{cases} P, & \text{for} \quad 0 \le P < 0.90 \\ 0.13P + 0.78, & \text{for} \quad 0.90 \le P < 3.91 \\ 0.084P + 0.96, & \text{for} \quad 3.91 \le P \end{cases}. \tag{4}$$

3.4. Leakage Losses Modeling

[22] Leakage losses were assumed to occur through gravitational flow [*Laio et al.*, 2001]. The leakage loss rate (Q) was assumed to be at its maximum for saturated soil moisture conditions. Q can be expressed using the hydraulic conductivity model proposed by *Brutsaert* [1968]:

$$Q = K_s \Theta^{\beta}, \tag{5}$$

where K_s is the saturated hydraulic conductivity (mm d^{-1}) and β the fitted parameter. The parameters K_s and β were estimated using nonlinear least squares regression between s calculated from equation (1) and observed s. On the basis of our regression analysis, we obtained a K_s of 35.6, typical for loam and sandy loam, and β of 5.8, typical for wet sandy clay loam and dry clay [*Campbell and Norman*, 1998].

[23] Finally, given the large precipitation intensity in this region, it is necessary to resolve whether the infiltration process is supply or soil controlled. On a daily time step, it is reasonable to assume that ponding occurs when rainwater input (e.g., throughfall plus stemflow) to the soil surface exceeds the soil infiltration capacity (SIC). Hence, when $P - I_c$ exceeds SIC, which to a first order can be approximated by K_s, ponding occurs and the infiltration rate is set to K_s. On short timescales (e.g., minutes to hours), both sorptivity (S_p; mm $min^{-0.5}$) and K_s (mm min^{-1}) are needed to describe SIC (mm min^{-1}) [e.g., *Philip*, 1957], given by

$$\mathrm{SIC} = K_s + \frac{1}{2} S_p t^{-1/2} \tag{6}$$

As time progresses, the sorption effect diminishes and SIC approaches K_s. It is clear that K_s sets the lower limit on SIC; it also becomes the more appropriate measure of SIC for long duration. Since the integration time step is large (e.g., daily), the simplest approximation is to neglect the contribution of sorption to SIC. Furthermore, we note that throughfall and stemflow are both calibrated with respect to daily rainfall data, and hence, can be used on a daily time step for these ponding calculations (despite the point-process approximation for precipitation).

[24] The ponded water in the next day (or time step) is first computed by including any new water input to the surface (i.e., $P - I_c$ at the present time step) plus the ponded water in the previous day (i.e., $P - I_c - K_s$ at the previous time step), and then is permitted to infiltrate the soil surface at rate identical to K_s. This process is repeated until the "supply" of water limits the infiltration process (i.e., no ponding). We note that this infiltration approach differs from the standard generation of ponding approach used by *Rodriguez-Iturbe et al.* [1999], *Laio et al.* [2001], and *Porporato et al.* [2002] which adopts the storage capacity of the root-zone rather than the infiltration capacity of the soil.

[25] When testing the model, measured precipitation time series can be used to drive the calculations. However, for future climate simulations, a synthetic precipitation time series must be constructed and is described next.

3.5. Simulations of Precipitation

[26] Two rainfall time series were constructed using random numbers generated from probability distributions representing current and future rainfall characteristics at the site. The rainfall characteristics were taken from rainfall records collected in 1968–2001 and future precipitation scenarios were taken from GCM output (details described later) for 2070–2100. As a result, two time series (i.e., the 1968–2001 and the 2070–2100) of each hydrological component can be computed. From the simulated time series of each hydrologic component, probability distributions for the period 1968–2001 and 2070–2100 can then be calculated. Shifts in the probability distributions of these hydrological components can then be readily related to shifts in the precipitation statistics.

[27] The frequency and amounts of rainfall events may be assumed to be stochastic variables with interval between precipitation events, τ (day), expressed as an exponential distribution given by:

$$f_T(\tau) = \lambda \exp(-\lambda\tau), \quad \text{for} \quad \tau \ge 0, \tag{7}$$

where $1/\lambda$ is the mean interval times (day). The amount of rainfall when rainfall occurs (mm) is also assumed to be an independent random variable, expressed by an exponential probability density function [*Laio et al.*, 2001]:

$$f_H(h) = \frac{1}{\eta} \exp\left(-\frac{1}{\eta} h\right), \quad \text{for} \quad h \ge 0, \tag{8}$$

where η is the mean depth of rainfall events (mm).

[28] Parameters $1/\lambda$ and η were determined using the rainfall characteristics at this site for the 1968–2001 and the 2070–2100 rainfall scenarios. For the 1968–2001 rainfall scenario, a long-term data record obtained at Miri Airport (4°19′N, 113°59′E) was used to assess the descriptive skill of the above precipitation model.

[29] A number of transient climate GCM simulations from the Hadley Centre for Climate Prediction and Research, available through a public website, were used. The 2070–2100 rainfall scenario at coordinates (2°30′–5°N, 112°30′–116°15′E) was constructed from the HadCM3 run [e.g., *Gordon et al.*, 2000]. The HadCM3 run assumes that future emissions of greenhouse gases will follow the IPCC-IS92a scenario [*Houghton et al.*, 1992], in which the atmospheric concentration of carbon dioxide increases by about 1% per year. The Hadley Centre offers climate change predictions formulated as differences between current climate, conventionally defined as 1960–1990, and the climate at the end of the 21st century, taken to be 2070–2100. We used average precipitation changes in the period 2070–2100 for each of the four seasons December-February (DJF), March-May (MAM), June-August (JJA) and September-November (SON) and obtained average rainfall in periods 1968–2001 and 2070–2100, respectively, for each season (Table 1). The Hadley Centre projected precipitation shifts for this region (i.e., comparing the climate in 1968–2001 with the climate in 2070–2100) are drier DJF (~180 mm), little change in MAM

Table 1. Rainfall Parameters for All Scenarios[a]

Scenario	Parameter	DJF	MAM	JJA	SON
2001–2002[b]	Average rainfall (mm/d)	4.92	5.13	3.85	9.73
2001–2002[b]	$1/\lambda$ (day)	1.76	2.12	2.16	1.42
2001–2002[b]	η (mm)	8.7	10.9	8.23	13.8
1968–2001[c]	Average rainfall (mm/d)	8.37	5.85	7.70	9.72
1968–2001[c]	$1/\lambda$ (day)	1.73	2.12	1.82	1.57
1968–2001[c]	η (mm)	14.5	12.0	14.1	15.3
2070–2100[d]	Average rainfall (mm/d)	6.37	5.65	8.45	11.22
A[e]	$1/\lambda$ (day)	2.28	2.12	1.67	1.36
B[f]	η (mm)	10.9	12.1	15.6	17.6

[a]See equations (7) and (8). DJF, December–January–February; MAM, March–April–May; JJA, June–July–August; SON, September–October–November.
[b]Average annual rainfall is 2154.4 mm.
[c]Average annual rainfall is 2884.4 mm.
[d]Average annual rainfall is 2888.5 mm.
[e]Values of η are the same as in the 1968–2001 scenario.
[f]Values of $1/\lambda$ are the same as in the 1968–2001 scenario.

(~20 mm), wetter JJA (~70mm), and wetter SON (~140 mm). Parameters $1/\lambda$ and η in the 2070–2100 scenario were obtained, according to two hypotheses, using the total amount of rainfall P (mm) for each season using

$$P = D_{season}\eta\lambda, \tag{9}$$

where D_{season} is the number of days in each season (day).

[30] We constructed two types of scenarios for 2070–2100 (Table 1). Scenario 2070–2100 A which computes $1/\lambda$ for the 2070–2100 precipitation but retains η for 1968–2001. Scenario 2070–2100 B which computes η for 2070–2100 but retains $1/\lambda$ as in 1968–2001. In other words, scenarios 2070–2100 A and B assume that future changes in rainfall are caused by either changes in rainfall frequency or rainfall depth. In reality, changes in precipitation are due to both frequency and depth. However, for simulation purposes, it is more constructive to evaluate the two "end-members" of the mechanisms causing precipitation shifts by assigning the entire shift to be either frequency or depth. Also, for the purposes of simulation, we assume that a single storm event does not exceed a day, and that plural storm events during a day can be lumped together as a single daily storm. This assumption is necessary as interception losses are related to daily precipitation thereby forcing the minimum time step of integration to be daily. We note that such a simplifying assumption may be reasonable here because single storm events exceeding one day seldom occur at least in the historical record at Miri Airport. However, before discussing these simulations, we evaluate the predictive skills of the simplified hydrologic model next.

4. Results and Discussion

4.1. Validation of the Water Cycling Model

[31] Figure 4 compares the transpiration rate calculated from equations (3a), (3b) and (3c) to measurements. Transpiration values calculated from equation (3a) reproduce best the measurements (in a root-mean squared sense). Calculations using equation (3b) systematically underestimate the measurements for small transpiration rates ($T_{r\_measured} < 2$ mm d^{-1}) because of the high sensitivity of α on Θ for low Θ (see Figure 2). This implies that the vegetation water stress if occurred at the minimum soil moisture content during the measurement period was not significantly large because the available energy still seems to be the over-riding factor on transpiration. When equation (3c) is used, the scatter between measured and modeled transpiration increases. Hence equation (3a) appears to be the best estimator of α and is adopted throughout.

[32] Daily variations of calculated soil moisture content and transpiration rate (for α in equation (3a)) forced by measured net radiation and precipitation are compared against measurements for DOY 78 (19 March) 2001 to DOY 151 (31 May) 2002 in Figure 5. The model well reproduces measured soil moisture content and transpiration rates despite all the simplifying assumptions. Figure 6 further compares calculated soil moisture content and daily transpiration rate against measurements, but here, transpiration rate measured during rainfall events were discriminated because water vapor flux measurements in days when rainfall occurred included evaporation from the wet canopy.

[33] It is logical to expect that future precipitation changes will lead to radiation changes because of increased or decreased cloud cover. Given that net radiation is the most critical factor for modeling transpiration here, a relationship between net radiation and precipitation must be developed to assess how future rainfall patterns alter the water cycle. We investigated three types of relationships between rainfall (P: mmd^{-1}) and net radiation (R_n: Wm^{-2}) as follows: (1) R_n was a constant value obtained by averaging R_n over the measurement period (R_n = 136.1). (2) The regression line described by an exponential model was fitted to R_n against P ($R_n = 147.4 \exp(-0.0136\,P)$, $R^2 = 0.22$). (3) R_n values related to P were obtained as random numbers generated by Gaussian representing the distributions of R_n in each bin range of P, that is, $0 \le P < 10$ (μ = 145.0, σ = 33.7), $10 \le P < 20$ (μ = 108.8, σ = 4.8) and $20 \le P$ (μ = 92.3, σ = 22.4) (where μ and σ are the mean and the standard deviation, respectively). Figure 7 compares probability distribution functions of transpiration rate ($p(T_r)$) and soil moisture content ($p(s)$) calculated using measured R_n to

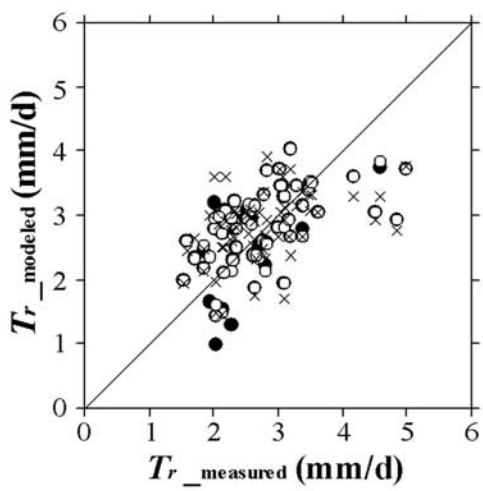

Figure 4. Comparison between measured ($T_{r\_measured}$) and modeled transpiration rate ($T_{r\_modeled}$). The model transpiration uses α from equations (3a) (open circle), (3b) (solid circle), and (3c) (cross).

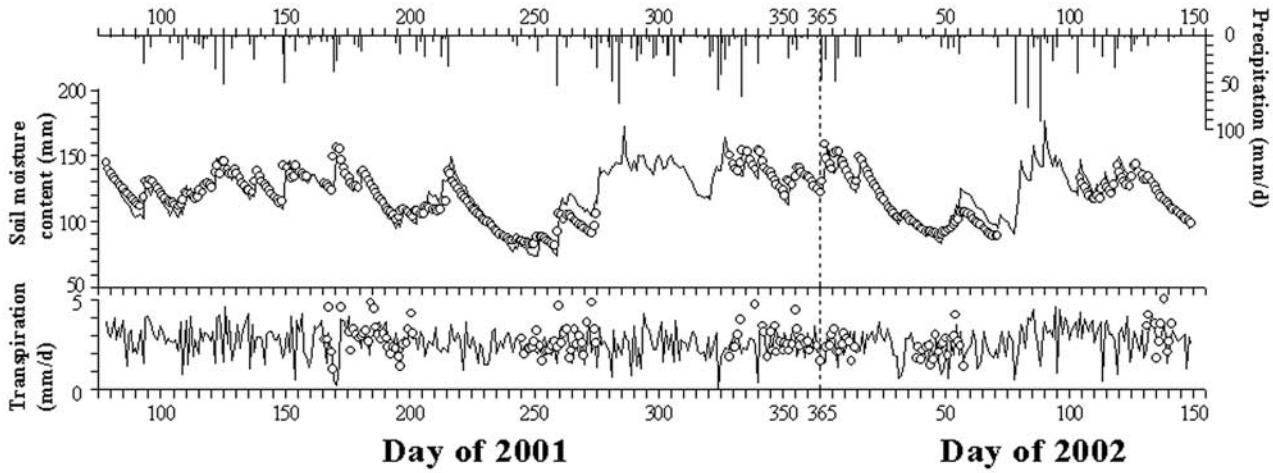

Figure 5. (top) Total daily precipitation (bars, right scale), (middle) measured (circle) and calculated (line) daily average soil moisture content (left scale), and (bottom) measured (circle) and calculated (line) transpiration rate (left scale) for the measurement period, DOY 78 (19 March) 2001 to DOY 151 (31 May) 2002.

those calculated using the above three methods. Mean values of transpiration rate calculated by all three methods were almost identical. Furthermore, the computed probability distributions of soil moisture content for all three methods were almost identical. However, the probability density function of transpiration suggests that method 3 appears to best reproduce the measured ($p(T_r)$) especially at the tails.

[34] Given that the projected GCM precipitation statistics are provided at seasonal timescales, it is instructive to compare how well the measured and modeled $p(s)$ agree in 2001–2002 for all four seasons (Figure 8). We included the computed $p(s)$ for the ensemble record of 1968–2001 (see Table 1) as reference. The comparisons between modeled and measured $p(s)$ for DJF, MAM, and JJA suggest that the model well reproduce seasonal dynamics in $p(s)$. We also compared the modeled $p(s)$ for DJF, MAM, JJA, and SON for both–the 2001–2002 observation period and the 1968–2001 period. Note that for MAM in 1968–2001 and 2001–2002 which have similar rainfall (see Table 1), $p(s)$ is about the same. Departures in Figure 8 for the DJF and JJA $p(s)$ are primarily due to the frequent droughts in 2001–2002 (i.e., flatter tails) when compared to ensemble record of 1968–2001 (see Table 1).

[35] In summary, the model estimated annual transpiration (T_r) and interception (I_c) in 2001–2002 to be 945.7 mm and 357.3 mm, respectively, suggesting that I_c can be up to 40% of (Table 2). The ratio of I_c to total P was 17%. Evapotranspiration, computed as the sum of T_r and I_c, was 1303.0 mm, accounting for about 60% of total P. Evapotranspiration studies by *Bruijinzeel* [1990] for humid tropical forests suggests that (1) annual T_r was, on average, 1045 mm (range 885–1285 mm), (2) I_c was, on average, 13% of incident P (range between 4.5 to 22%), and (3) annual evapotranspiration ranged from 1310 to 1500 mm. Our values for evapotranspiration and intercep-

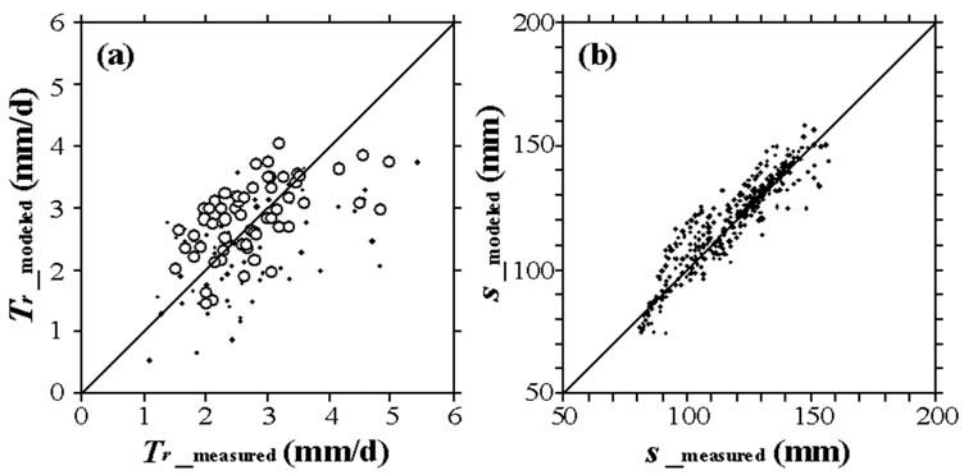

Figure 6. Comparisons between measured and modeled (a) transpiration rate for dry canopy (open circle) and wet canopy (solid circle) and (b) soil moisture.

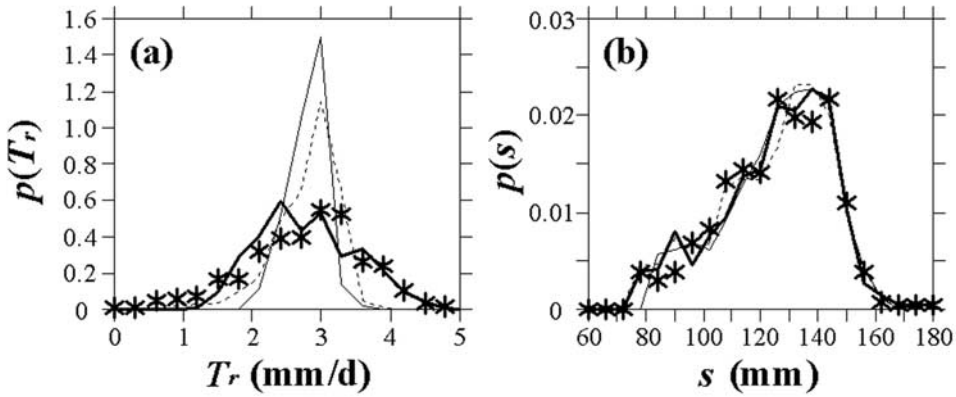

Figure 7. Probability density functions of (a) transpiration rate ($p(T_r)$) and (b) soil moisture content (p(s)) calculated using net radiation values from the measurements (asterisk), the average net radiation over the calculation period (thin solid line), the regression of the rainfall and the net radiation data (dashed line), and the random numbers generated by relationship between the rainfall and the net radiation data (thick solid line). Calculation period was the same as in Figure 5.

tion losses are comparable to those reported values. Although the majority of net radiation (R_n) was transformed to latent heat (LE) (72–86%), seasonal variations in LE existed and positively correlated with P. Total daily LE for dry periods DJF and JJA were 8.04 and 8.22 MJ m^{-2} d^{-1}, respectively, while daily LE for wet periods MAM and SON were 8.98 and 9.53 MJ m^{-2} d^{-1}, respectively. Our LE for the dry and wet periods correspond to LE measurements collected during the transition and the wet seasons in the Amazonian tropical forest [*Vourlitis et al.*, 2002], respectively. Having verified that the model partitions precipitation reasonably well into the different hydrologic reservoirs and fluxes, we proceed to discuss the seasonal water cycle and assess how future climatic shifts in precipitation regimes alter this partitioning.

4.2. Hydrologic Balance for Current and Future Precipitation Scenarios

[36] The hydrologic components of the study period 2001–2002 and scenarios 1968–2001, 2070–2100A and 2070–2100B (see Table 1; hereinafter referred to as 1968, A and B, respectively) for each of the four seasons are summarized in Tables 2 and 3, respectively. For the study period (2001–2002), we found that DJF and JJA were dryer, and MAM and SON were comparable to the 1968 scenario. As a result, annual precipitation (P) in 2001–2002 was about 730 mm less than the 1968 scenario. There were little changes in all the hydrologic components for MAM and JJA under all scenarios (1968, A and B) because P did not vary appreciably (Table 3). Total T_r for DJF, SON, and consequently, the entire year was not significantly altered by shifts in P. The computed ratio LE/R_n are 0.86 in DJF and 0.90 in SON for the 1968 (or present-day) scenario. This ratio was reduced to 0.77 and 0.80 in DJF and increased to 0.97 and 0.94 in SON for future scenarios A and B, respectively. Hence, the year total LE/R_n for all the scenarios were about the same.

4.3. Stochastic Representations of Hydrologic Components From the Scenarios

[37] Ensemble seasonal and annual probability distributions of the three hydrologic fluxes (T_r, I_c, Q) for scenarios

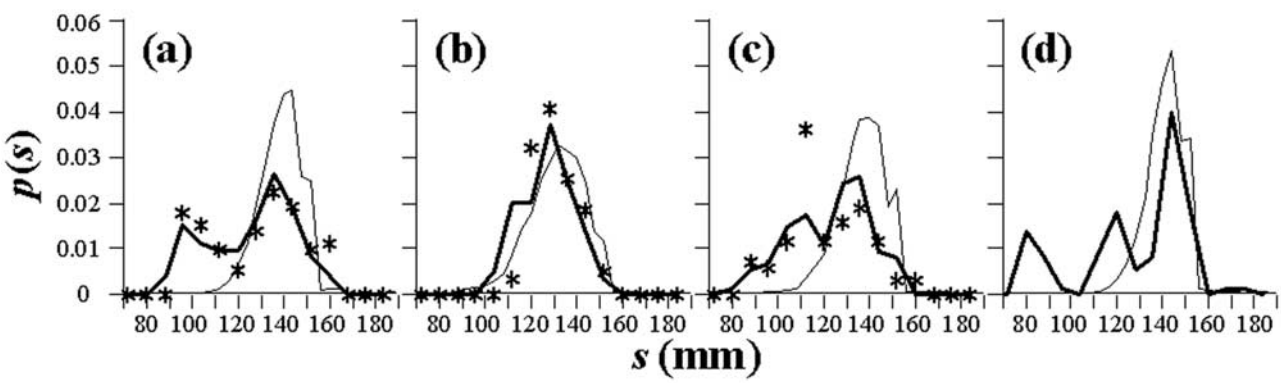

Figure 8. Probability density functions of soil moisture content (p(s)) for the same period as in Figure 5, estimated from actual soil moisture data (asterisk) and calculated by the model (thick line). (a) DJF, (b) MAM, (c) JJA, and (d) SON (see Table 1). Thin lines represent p(s) estimated from calculation results using the 1968–2001 scenario.

Table 2. Seasonal and Annual Water Balance for the Measurement Period 2001–2002

	P, mm	T_r,[a] mm	I_c,[a] mm	Q,[a] mm	R_n, MJ/m^{2}d	LE,[a,b] MJ/m^{2}d	LE/R_n
DJF	443.0	216.4	80.5	180.7	10.86	8.04	0.74
MAM	472.4	262.2	77.3	131.4	12.56	8.98	0.72
JJA	354.0	243.9	66.8	110.8	12.08	8.22	0.68
SON	885.0	223.2	132.7	450.4	11.09	9.53	0.86
Year total	2154.4	945.7	357.3	873.3	11.60	8.68	0.75

[a]Calculated using the water cycling model with measured climatic data.
[b]Latent heat flux.

1968, A and B as well as stored water are compared in Figures 9 and 10, respectively.

[38] On annual timescales, the shift in precipitation statistics did not alter the probability distributions of T_r, I_c, Q, and s (for either future scenario). Much of the alterations were observed at seasonal timescales. Figure 9 suggests that T_r is the most robust to shifts in rainfall. A change in precipitation alters both soil moisture (which influences α) and radiation inputs (through cloud cover). Increases in rainfall increase soil moisture (and hence α) but decrease R_n thereby introducing some cancellation.

[39] Decrease in rainfall amount in DJF reduced interception losses under both scenarios A and the B (Table 3 and Figure 9, plot a-2). For scenario A, the more frequent light rainfall events were almost perfectly intercepted by the canopy, while under scenario B, the heavier (though less frequent storms) increased I_c (Figure 9, plot d-2).

[40] The canonical structure of the probability density function of Q was a bimodal distribution reflecting the "two-states" of drainage – either large after a precipitation or very small in the absence of precipitation. Decrease in rainfall amount increase contributions to low Q (<5.0 mm d^{-1}) and decrease the high Q (35.0–40.0 mm d^{-1}) (Figure 9, plot a-3). Owing to a reduction in heavy rainfall events in scenario B, the upper Q tails are significantly reduced in scenario B. Also, for SON, an increase in heavy rainfall event in scenario B appreciably increases the upper Q tails. All hydrologic components had little changes in MAM and JJA where GCM projections suggest little changes (Figure 9, plots b-1, b-2, b-3, c-1, c-2, and c-3).

[41] As a result all hydrologic components for total year experienced little change for both scenarios because decrease in rainfall amounts for DJF were compensated for by increases in SON (Figure 9, plots e-1, e-2, and e-3).

[42] Figure 10 shows the seasonal and annual probability distributions of soil moisture content $p(s)$ for the two scenarios (see Table 1). Decrease in heavy rainfall under scenario B does not affect $p(s)$, while decrease in rainfall frequency increases the dry mode (Figure 10a). Again, some partial cancellations emerge; for example, storms with smaller (but more frequent) depths are likely to be intercepted; however, storms with bigger depths (but less frequent) contribute to the drainage. Hence, the soil moisture content probability density function appears more robust to future shifts in precipitation when compared to interception or drainage.

5. Conclusions

[43] Using a combination of field measurements, simplified water balance model, and GCM projections of precipitation, we examine how future shifts in precipitation affect water reservoirs and fluxes with an Asian tropical rain forest. The field measurements permitted us to derive key relationships that tie the "forcing" term with parameters or state variables. For example, the field data were used to derive relationships between precipitation and net radiation variability, between transpiration and extractable water content, between precipitation and interception, and the drainage flow parameters. The Hadley Centre projected precipitation shifts for this region in 2070–2100 are drier DJF, little change in MAM, wetter JJA, and wetter SON compared to the climate in 1968–2001. We assumed that this shift occurs in one of the two ways: change in precipitation depth or change in precipitation frequency. In reality, both frequency and depth are likely to change; however, by exploring the "end-members" of the precipitation shift, we can quantify the likely changes in hydrologic fluxes and reservoirs. We found that shifts in precipitation primarily impacts the probability distribution of interception, followed by drainage fluxes. The transpiration and soil moisture probability were least impacted by shifts in precipitation. This, in part, is attributed to the fact

Table 3. Seasonal and Annual Water Balance for All Three Scenarios[a]

	Scenario	P, mm	T_r, mm	I_c, mm	Q, mm	R_n, MJ/m^{2}d	LE,[b] MJ/m^{2}d	LE/R_n
DJF	1968–2001	753.3	248.1	111.7	397.7	11.38	9.73	0.86
DJF	2070–2100A	573.3	246.1	83.5	254.8	11.65	8.91	0.77
DJF	2070–2100B	573.3	248.4	95.8	239.8	11.63	9.31	0.80
MAM	1968–2001	538.2	251.1	85.0	210.7	11.71	8.89	0.76
MAM	2070–2100A	519.8	251.4	83.3	185.7	11.75	8.86	0.75
MAM	2070–2100B	519.8	250.1	83.3	191.0	11.74	8.83	0.75
JJA	1968–2001	707.8	253.8	106.7	337.5	11.52	9.54	0.83
JJA	2070–2100A	776.8	254.1	117.2	397.6	11.40	9.83	0.86
JJA	2070–2100B	776.8	253.2	112.7	398.9	11.43	9.69	0.85
SON	1968–2001	884.5	252.1	128.8	500.9	11.30	10.19	0.90
SON	2070–2100A	1021.0	248.7	150.4	618.3	11.04	10.68	0.97
SON	2070–2100B	1021.0	250.4	140.6	626.6	11.14	10.47	0.94
Year total	1968–2001	2883.8	1005.0	432.1	1446.8	11.48	9.59	0.84
Year total	2070–2100A	2890.9	1000.2	434.4	1456.4	11.46	9.57	0.84
Year total	2070–2100B	2890.8	1000.2	432.4	1456.4	11.48	9.57	0.83

[a]See Table 1.
[b]Latent heat flux.

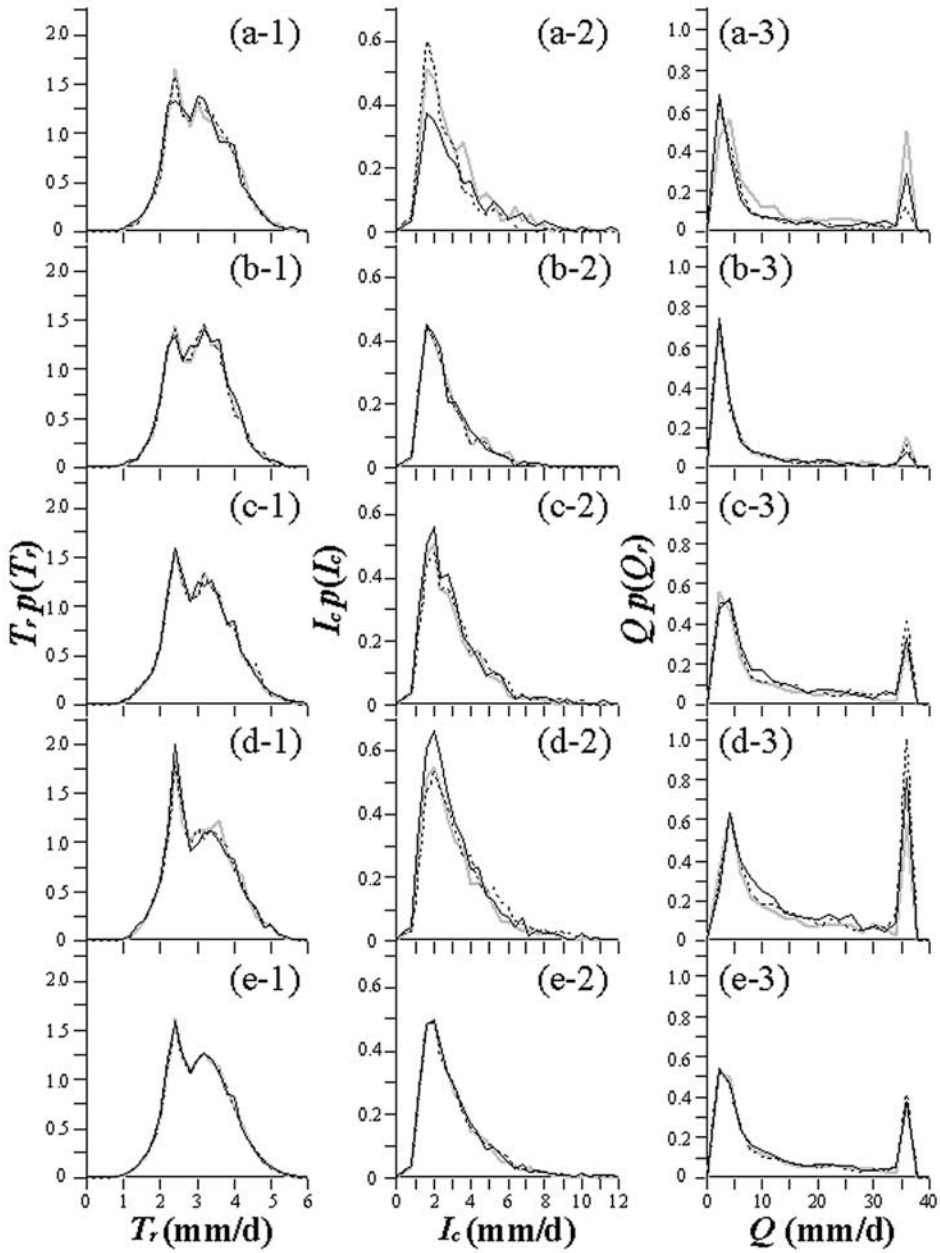

Figure 9. Probability density functions of the hydrologic fluxes for scenarios 1968–2001 (shaded solid line), 2070–2100A (thin solid line), and 2070–2100B (dashed line) (see Table 1). Left panels show transpiration rate (T_r), middle panels show interception (I_c), and right panels show leakage losses (Q). Reading from the top graph: each graph corresponds to DJF, MAM, JJA, SON (see Table 1), and whole year.

that smaller depth (but more frequent) precipitation events are efficiently intercepted by the ecosystem; while larger depth (but less frequent) precipitation events increase primarily the drainage. Increased precipitation (and hence increased soil moisture) was compensated for by reduced radiation resulting in little overall change in the probability distribution of transpiration.

[44] This study primarily focused on precipitation shifts and its propagation through water fluxes and reservoirs; however, in reality, numerous other factors must be considered. For example, the effects of increasing atmospheric carbon dioxide on transpiration and leaf area must be accounted for in future studies. Preliminary evidence from a Free Air CO_2 Enrichment (FACE) experiment in a southeastern United States hardwood forest suggests that increasing atmospheric carbon dioxide reduces T_r [e.g., *Wullschleger and Norby*, 2001] through a reduction in stomatal conductance [e.g., *Lockwood*, 1999]. Furthermore, increase in atmospheric CO_2 can increase I_c by increasing LAI [e.g., *Lichter et al.*, 2000].

[45] On much longer timescales, increase in atmospheric CO_2 can induce higher soil water holding capacity because

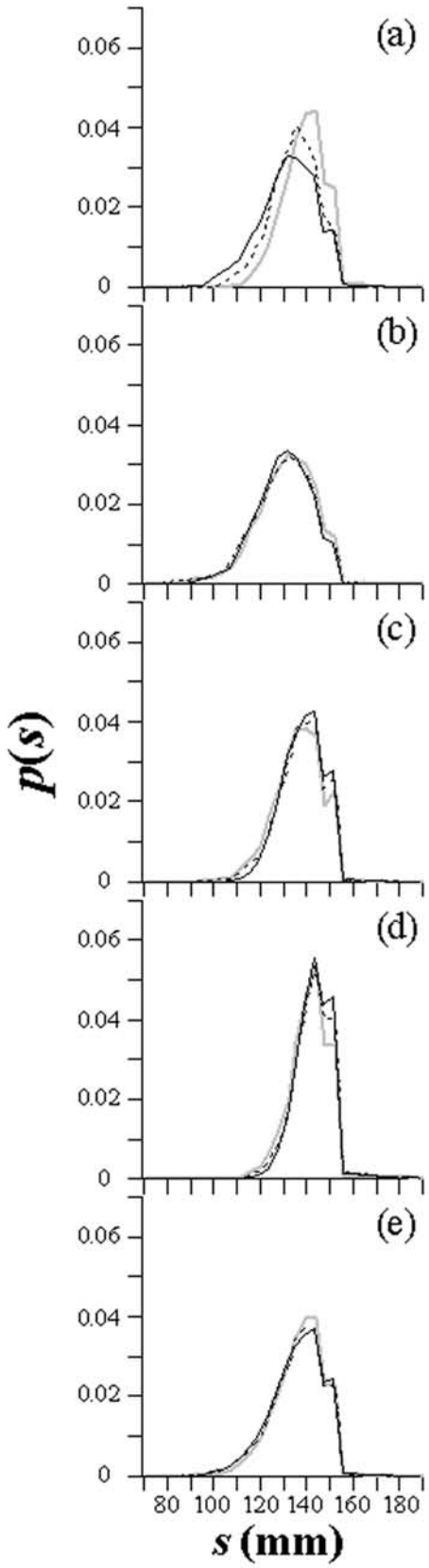

Figure 10. Same as Figure 9 but for soil moisture content.

of an increase in soil organic matter content resulting from increased litter production [e.g., *Nicklaus et al.*, 1998; *Schäfer et al.*, 2002]. Other FACE experiments, however, conducted in the southeastern United States on a 14-year-old pine plantations suggest that LAI, stomatal conductance, and bulk canopy conductance are, to a first order, unaltered by elevated atmospheric CO_2 [*Schäfer et al.*, 2002]. Hence tracking the precise effects of elevated atmospheric CO_2 on leaf area and transpiration rates for these Southeast Asian rain forests remains an open question and requires extensive and technically difficult experiments.

[46] **Acknowledgments.** We thank Hua Seng Lee and Lucy Chong, of Forest Research Center, Forest Department of Sarawak, for providing the opportunity for this study. This work has been supported by CREST (Core Research for Evolutional Science and Technology) of JST (Japan Science and Technology) and a grant from the Ministry of Education, Science and Culture of Japan (#13760120). We thank the leader, Tohru Nakashizuka for his support and the many colleagues who helped us with this work. Gabriel Katul acknowledges support from Duke University's Center on Global Change, the National Science Foundation (NSF-EAR and NSF-DMS), and the Department of Energy through their Biological and Environmental Research (BER) Program, the Southeast Regional Center (SERC) of the National Institute for Global Environmental Change (NIGEC), and the DOE Terrestrial Carbon Processes Program (TCP) and the FACE project.

References

Bruijnzeel, L. A. (1990), Hydrology of moist tropical forests and effects of conversion: A state of knowledge review, Int. Hydrol. Programme, United Nations Educ., Sci., and Cultural Organ., Paris.

Brutsaert, W. (1968), The permeability of a porous medium determined from certain probability laws for por size distribution, *Water Resour. Res.*, *4*, 425–434.

Campbell, G. S., and J. M. Norman (1998), *An Introduction to Environmental Biophysics*, 2nd ed., Springer-Verlag, New York.

Choudhury, B., N. E. DiGirolamo, J. Susskind, W. L. Darnell, S. K. Gupta, and G. Asrar (1998), A biophysical process-based estimate of global land surface evaporation using satellite and ancillary data, II. Regional and global patterns of seasonal and annual variations, *J. Hydrol.*, *205*, 186–204.

De Bruin, H. A. R. (1983), A model for the Priestly-Taylor parameter α, *J. Clim. Appl. Meteorol.*, *22*, 572–578.

Dykes, A. P. (1997), Rainfall interception from a lowland tropical rainforest in Brunei, *J. Hydrol.*, *200*, 260–279.

Food and Agriculture Organization (1993), Forest resources assessment 1990—Tropical countries, *For. Pap. 112*, Rome.

Gordon, C., C. Cooper, C. A. Senior, H. Banks, J. M. Gregory, T. C. Johns, J. F. B. Mitchell, and R. A. Wood (2000), The simulation of SST, sea ice extents and ocean heat transports in a version of the Hadley Centre coupled model without flux adjustments, *Clim. Dyn.*, *16*, 147–168.

Grace, J., J. Lloyd, J. McIntyre, A. Miranda, P. Meir, H. Miranda, J. Moncrieff, J. Massheder, I. Wright, and J. Gash (1995), Fluxes of carbon dioxide and water vapour over an undisturbed tropical forest in south-west Amazonia, *Global Change Biol.*, *1*, 1–12.

Grace, J., Y. Malhi, N. Higuchi, and P. Meir (2001), Productivity of tropical forests, in *Terrestrial Global Productivity*, edited by J. Roy et al., pp. 401–426, Academic, San Diego, Calif.

Hodnett, M. G., L. P. da Silva, H. R. da Rocha, and R. C. Senna (1995), Seasonal soil water storage changes beneath central Amazonian rainforest and pasture, *J. Hydrol.*, *170*, 233–254.

Houghton, J. T., B. A. Callander, and S. K. Varney (Eds.) (1992), *Climate Change 1992: The Supplementary Report to the IPCC Scientific Assessment*, Cambridge Univ. Press, New York.

Houghton, J. T., Y. Ding, D. J. Griggs, M. Noguer, P. J. van der Linden, and D. Xiaosu (Eds.) (2001), *Climate Change 2001: The Scientific Basis*, Cambridge Univ. Press, New York.

Ishizuka, S., S. Tanaka, K. Sakurai, H. Hirai, H. Hirotani, K. Ogino, H.-S. Lee, and J. J. Kedawang (1998), Characterization and distribution of soils at Lambir Hills National Park in Sarawak, Malaysia, with special reference to soil hardness and soil texture, *Tropics*, *8*, 31–44.

Kelliher, F. M., R. Luening, M. R. Raupach, and E.-D. Schulze (1995), Maximum conductances for evaporation from global vegetation types, *Agric. For. Meteorol.*, *73*, 1–16.

Kumagai, T., T. M. Saitoh, Y. Sato, T. Morooka, O. J. Manfroi, K. Kuraji, and M. Suzuki (2004), Transpiration, canopy conductance and the decoupling coefficient of a lowland mixed dipterocarp forest in Sarawak, Borneo: Dry spell effects, *J. Hydrol.*, in press.

Laio, F., A. Porporato, L. Ridolfi, and I. Rodriguez-Iturbe (2001), Plants in water-controlled ecosystems: Active role in hydrologic processes and response to water stress, II. Probablistic soil moisture dynamics, *Adv. Water Res.*, *24*, 707–723.

Lean, J., and D. A. Warrilow (1989), Simulation of the regional climatic impact of Amazonian deforestation, *Nature*, *342*, 411–413.

Lichter, J., M. Lavine, K. A. Mace, D. D. Richter, and W. H. Schlesinger (2000), Throughfall chemistry in a loblolly pine plantation under elevated atmospheric CO_2 concentrations, *Biogeochemistry*, *50*, 73–93.

Lockwood, J. G. (1999), Is potential evapotranspiration and its relationship with actual evapotranspiration sensitive to elevated atmospheric CO_2 levels?, *Clim. Change*, *41*, 193–212.

Malhi, Y., E. Pegoraro, A. D. Nobre, M. G. P. Pereira, J. Grace, A. D. Culf, and R. Clement (2002), Energy and water dynamics of a central Amazonian rain forest, *J. Geophys. Res.*, *107*(D20), 8061, doi: 10.1029/2001JD000623.

Manfroi, O. J., K. Kuraji, N. Tanaka, M. Suzuki, M. Nakagawa, T. Nakashizuka, and L. Chong (2004), The stemflow of trees in a Bornean lowland tropical forest, *Hydrol. Processes*, in press.

Niklaus, P. A., D. Splinger, and C. Körner (1998), Soil moisture dynamics of calcareous grassland under elevated CO_2, *Oecologia*, *117*, 201–208.

Nobre, C. A., P. J. Sellers, and J. Shukla (1991), Amazonian deforestation and regional climate change, *J. Clim.*, *4*, 957–988.

Ohta, S., and S. Effendi (1992), Ultisols of "lowland dipterocarp forest" in east Kalimantan, Indonesia. II. Status for carbon, nitrogen, and phosphorous, *Soil Sci. Plant Nutr. Tokyo*, *38*, 207–216.

Paegle, J. (1987), Interactions between convective and large-scale motions over Amazonia, in *The Geophysiology of Amazonia*, edited by R. E. Dickinson, pp. 347–387, John Wiley, Hoboken, N. J.

Philip, J. R. (1957), The theory of infiltration.1. The infiltration equation and its solution, *Soil Sci.*, *83*, 345–357.

Porporato, A., P. D'Odorico, F. Laio, L. Ridolfi, and I. Rodriguez-Iturbe (2002), Ecohydrology of water-controlled ecosystems, *Adv. Water Res.*, *25*, 1335–1348.

Priestly, C. H. B., and R. J. Taylor (1972), On the assessment of surface heat flux and evaporation using large-scale parameters, *Mon. Weather Rev.*, *100*, 81–92.

Rodriguez-Iturbe, I., A. Porporato, L. Ridolfi, V. Isham, and D. R. Cox (1999), Probabilistic modelling of water balance at a point: The role of climate, soil and vegetation, *Proc. R. Soc. London, Ser. A*, *455*, 3789–3805.

Sakurai, K. (1999), Soils and agriculture in Borneo (in Japanese with English abstract), *Tropics*, *9*, 27–40.

Schäfer, K. V. R., R. Oren, C.-T. Lai, and G. G. Katul (2002), Hydrologic balance in an intact temperate forest ecosystem under ambient and elevated atmospheric CO_2 concentration, *Global Change Biol.*, *8*, 895–911.

Shuttleworth, W. J., et al. (1984), Eddy correlation measurements of energy partition for Amazonian forest, *Q. J. R. Meteorol. Soc.*, *110*, 1143–1162.

Skole, D., and C. Tucker (1993), Tropical deforestation and habitat fragmentation in the Amazon: Satellite data from 1978 to 1988, *Science*, *260*, 1905–1910.

Vourlitis, G. L., N. Priante Filho, M. M. S. Hayashi, J. de S. Nogueira, F. T. Caseiro, and J. H. Campelo Jr. (2002), Seasonal variations in the evapotranspiration of transitional tropical forest of Mato Grosso, Brazil, *Water Resour. Res.*, *38*(6), 1094, doi: 10.1029/2000WR000122.

Webb, E. K., G. I. Pearman, and R. Leuning (1980), Correction of flux measurements for density effects due to heat and water vapour transfer, *Q. J. R. Meteorol. Soc.*, *106*, 85–100.

Wood, E. F., D. P. Lettenmaier, and V. G. Zartarian (1992), A land-surface hydrology parameterization with subgrid variability for general circulation models, *J. Geophys. Res.*, *97*(D3), 2717–2728.

Wullschleger, S. D., and R. J. Norby (2001), Sap velocity and canopy transpiration in a sweetgum stand exposed to free-air CO_2 enrichment (FACE), *New Phytol.*, *150*, 489–498.

Yamakura, T., M. Kanzaki, A. Itoh, T. Ohkubo, K. Ogino, E. O. K. Chai, H.-S. Lee, and P. S. Ashton (1995), Forest architecture of Lambir rain forest revealed by a large-scale research plot, in *Reports of New Program for Promotion of Basic Sciences. Studies of Global Environmental Changes With Special Reference to Asia and Pacific Regions*, vol. II-3, *Long Term Ecological Research of Tropical Rain Forest in Sarawak, Ehime University, Japan, March 1995*, edited by H.-S. Lee et al., pp. 2–20, Ehime Univ., Matsuyama, Japan.

T. Ichie, Field Science Center for Northern Biosphere, Hokkaido University, Sapporo 060-0808, Japan.

G. G. Katul, Nicholas School of the Environment, Duke University, Durham, NC 27708, USA.

T. Kumagai, University Forest in Miyazaki, Kyushu University, Shiibason, Miyazaki 883-0402, Japan. (kuma@forest.kyushu-u.ac.jp)

K. Kuraji, O. J. Manfroi, T. Morooka, and M. Suzuki, Graduate School of Agricultural and Life Sciences, University of Tokyo, Tokyo 113-8654, Japan.

A. Porporato, Department of Civil and Environmental Engineering, Duke University, Durham, NC 27708, USA.

Y. Sato and T. M. Saitoh, Research Institute of Kyushu University Forest, Fukuoka 811-2307, Japan.